Enhancing the detection efficiency of condensation particle counters for sub-2 nm particles

Barmpounis, K.; Ranjithkumar, A.; Schmidt-Ott, A.; Attoui, M; Biskos, G.

DOI
10.1016/j.jaerosci.2017.12.005

Publication date
2018

Document Version
Final published version

Published in
Journal of Aerosol Science

Citation (APA)
Barmpounis, K., Ranjithkumar, A., Schmidt-Ott, A., Attoui, M., & Biskos, G. (2018). Enhancing the detection efficiency of condensation particle counters for sub-2 nm particles. *Journal of Aerosol Science*, *117*, 44-53. https://doi.org/10.1016/j.jaerosci.2017.12.005

Journal of Aerosol Science 117 (2018) 44–53

Contents lists available at ScienceDirect

Journal of Aerosol Science

journal homepage: www.elsevier.com/locate/jaerosci

Enhancing the detection efficiency of condensation particle counters for sub-2 nm particles

K. Barmpounis[a,b,*], A. Ranjithkumar[a], A. Schmidt-Ott[a], M. Attoui[c], G. Biskos[b,d]

[a] Faculty of Applied Sciences, Delft University of Technology, Delft 2628, BL, The Netherlands
[b] Energy Environment and Water Research Center, The Cyprus Institute, Nicosia 2121, Cyprus
[c] LISA, UMR CNRS 7583, Université Paris Est Creteil et Université Paris Diderot, Institut Pierre Simon Laplace, 61, av du Géneral de Gaulle, 94010 Créteil Cedex, France
[d] Faculty of Civil Engineering and Geosciences, Delft University of Technology, Delft 2628, CN, The Netherlands

ABSTRACT

The detection efficiency of Condensation Particle Counters (CPCs) reduces drastically as particle size becomes smaller than 2 nm. Increasing the supersaturation in order to enhance the detection efficiency, has limited applicability because the onset supersaturation value of droplet formation by homogeneous nucleation is very close to the heterogeneous onset supersaturation for sub-2 nm particles. In this work we introduce a new method for increasing the detection efficiency of CPCs for sub-2 nm particles, which relies mainly on controlling the spatial distribution of the supersaturation profile by simply modifying the operating temperatures of the CPC. We evaluated the new method by generating monodisperse particles in the size range of 0.98–4.50 nm and used them to characterize a TSI 3025 CPC. We achieved significant increase of the detection efficiency for sub-2 nm particles. Furthermore, we calculated the supersaturation field developed in the condenser tube with a finite element model and used it to determine the detection efficiency according to heterogeneous nucleation theory. These calculations reveal that the observed increase of the detection efficiency can be explained by the manipulation of the spatial distribution of the supersaturation field. The method introduced here can greatly improve the detection efficiency of CPCs and in the meantime further extend their use for particle sizing purposes in the sub-2-nm range.

1. Introduction

Observations of nucleation events in the atmosphere are important for better understanding the physical processes governing the evolution of the size distribution of aerosol particles, and thus for improving the predictability of climate models. In these observations, measurements of the concentration of particles smaller than 2 nm are of particular importance for understanding the early stages of particle formation and their subsequent growth. Due to their highly diffusive nature, however, the detection of particles having sizes in that range can be challenging, especially in the context of atmospheric observations where their concentrations can be relatively low (Kulmala et al., 2013).

Condensation Particle Counters (Agarwal & Sem, 1980; Bricard, Delattre, Madelaine, & Pourprix, 1976; McMurry, 2000; Stolzenburg & McMurry, 1991) have been widely used for measuring the concentration of airborne nanoparticles. Compared to an aerosol electrometer (Liu, Whitby, & Pui, 1974), CPCs have an extremely high counting sensitivity because, in principle, they have

* Corresponding author at: Faculty of Applied Sciences, Delft University of Technology, Delft 2628, BL, The Netherlands.
E-mail address: k.barmpounis@lemonlabs.eu (K. Barmpounis).

https://doi.org/10.1016/j.jaerosci.2017.12.005
Received 20 January 2017; Received in revised form 27 October 2017; Accepted 15 December 2017
Available online 18 December 2017
0021-8502/

the capability of single-particle detection. In addition, CPCs are unique detectors of uncharged particles, a fact that is especially valuable for studies of the atmospheric aerosol (Kulmala et al., 2004).

One limitation of CPCs is that their detection efficiency decreases substantially when particle size decreases below a threshold value. Smaller particles require a higher supersaturation in order to initiate condensational growth, because the equilibrium vapor pressure over a curved surface is higher than that over a flat surface (Kelvin effect). The 50% detection efficiency of standard CPCs is ca. 10 nm (e.g., for the TSI Model 3010). A recent study has shown that by modifying the operating conditions of the TSI Model 3772, detection of sub-2 nm particles is possible with surprisingly high detection efficiency (Kangasluoma et al., 2015). In the case of ultrafine CPCs, the 50% detection efficiency is achieved for particles having sizes close to 2.5 nm e.g. TSI Models 3025 and 3776; (Kuang, Chen, McMurry, & Wang, 2012; Stolzenburg & McMurry, 1991). Parallel to these developments, state-of-the-art aerosol classifiers can already size sub-2 nm particles and atomic clusters with extremely high resolution (De Juan, & Fernández de la Mora, 1998; Maisser et al., 2015; Rosser & Fernández de la Mora, 2005; Rus et al., 2010). As a result, CPCs with higher detection efficiencies than those of commercial systems are needed for integrating them in spectrometers capable of measuring the size distributions of particles in the sub-2 nm range.

A number of studies have looked into further increasing the detection efficiency of CPCs leading to the development of several instruments able to detect particles in the sub-2 nm range (Iida, Stolzenburg, & McMurry, 2009; Kulmala et al., 2007; Lehtipalo, Sipilä, Riipinen, Nieminen, & Kulmala, 2009; Mordas et al., 2005; Saghafifar et al., 2009; Seto, Okuyama, De Juan, & de la Mora, 1997; Sgro & Fernández de la Mora, 2004; Sipilä et al., 2009; Mikko Sipilä et al., 2008; Vanhanen et al., 2011). A common feature in many studies is that the detection efficiency of a CPC is enhanced by augmenting the temperature difference between the saturator and the condenser tube (Hermann & Wiedensohler, 2001; Kuang et al., 2012). Increasing the temperature difference increases the supersaturation in the condenser tube, which in turn increases the activation probability of the smaller particles. Other studies have focused on the use of working fluids other than butanol, aiming to take advantage of their different physical behavior during nucleation (Magnusson, Koropchak, Anisimov, Poznjakovskiy, & de la Mora, 2003). Iida et al. (2009) pointed out that an ideal working fluid for activation of small ions should have a high surface tension and low vapor pressure.

In thermally diffusive laminar flow CPCs, the supersaturation profile developed inside the condenser has a non-uniform spatial distribution with values ranging from 1 (i.e. saturation) up to some maximum value determined by the operating conditions of the instrument. Given that particles follow a convective-diffusive trajectory inside the condenser, a certain fraction of their population will not traverse regions at which the supersaturation is high enough for activation. Controlling the spatial distribution of the supersaturation profile could increase the fraction of particles traversing regions where they can activate, thereby providing a new way of increasing the particle activation probability and therefore the detection efficiency of CPCs.

In this article, we introduce a new controlling parameter for increasing the detection efficiency of continuous laminar flow CPCs, which relies on manipulating the spatial distribution of the supersaturation profile by taking advantage of the nonlinear dependence of the supersaturation on temperature. We call this new parameter temperature window (TW), defined by the location of the temperature difference between the saturator and condenser (ΔT) in the temperature domain. We have identified that for a given constant ΔT, variation of the spatial distribution of the supersaturation profile can be achieved by choosing different TWs. This variation was found to have significant impact on the detection efficiency of sub-2 nm particles. We tested different TWs on a butanol-based ultrafine CPC (TSI Model 3025) and report the measured detection efficiency for various particle sizes in the 0.94–4.5 nm mobility diameter range. In addition, we provide a theoretical explanation of the observed effect, using a simple model of the CPC detection efficiency.

2. Simulations

2.1. Background

The operating principle of CPCs relies on the exposure of the sampled particles to a supersaturated vapor (e.g. butanol), thereby initiating condensation of vapors on the surface of the particles. Three methods are used for creating the required supersaturation: 1. expansion of a saturated flow (Wagner, 1985), 2. mixing of cold and warm saturated flows (Kousaka, Niida, Okuyama, & Tanaka, 1982), and 3. thermally diffusive laminar flow cooling (Bricard et al., 1976; Stolzenburg & McMurry, 1991). The latter is applied in the majority of commercial CPCs, and thus the following discussion is restricted to this method. In order to create the required supersaturation, the sampled aerosol gets saturated in vapors by passing it through the saturator tube that contains the working fluid maintained at a constant temperature. The saturated flow then enters the condenser tube, which is maintained at a lower temperature than that of the saturator, in order to create the required temperature difference for supersaturation to occur. The condensing vapors increase the particle diameter to the micron size range, which can then be easily detected by optical methods (light scattering).

The detection efficiency η of a CPC is defined as the ratio of number concentration of the detected particles N_{CPC} over the total particle number concentration at the inlet of the CPC N_{total}:

$$\eta = N_{CPC}/N_{total}, \tag{1}$$

and depends primarily on the activation probability of particles, which is mainly a function of the supersaturation and the particle diameter. In addition, the chemical composition and the charge state of the particles (i.e. number of charges and polarity) has an important effect on their activation probability.

Diffusional particle losses inside the tubing of the CPC comprise another important process defining η, especially for particle sizes smaller than 2 nm. N_{total} is usually measured at the inlet of the CPC. As a result, the number of particles that reach the inlet of the

condenser tube is smaller than the N_{total} value measured at the inlet of the CPC. Both activation probability and diffusional particle losses inside the CPC are captured by our model and are discussed in the following subsections.

2.2. Particle activation probability

Particle growth by condensation occurs inside the condenser tube, in which a profile of supersaturated butanol vapor is developed as a result of the cooling of the incoming saturated flow. The saturation ratio S is defined as the ratio of partial vapor pressure P_{vap} over the equilibrium partial pressure $P_{sat,T}$ at any given gas temperature T:

$$S = P_{vap}/P_{sat,T}. \tag{2}$$

Particles passing through the condenser provide the necessary surface energy for heterogeneous nucleation. Vapor molecules then pass from the gas to the liquid phase via condensation on the surface of the particles, leading to the formation of larger droplets. Classical nucleation theory can be used to determine the droplet formation rate, resulting from heterogeneous nucleation, as follows (Fletcher, 1958):

$$J_{het} = J^0_{het}\exp(-\Delta G^*_{het}/k_b T). \tag{3}$$

Here ΔG^*_{het} is the formation free energy of the critical droplet size, k_b is the Boltzmann constant, T is the gas temperature and $J^0_{het} = \pi d_p^2 10^{29}$ is a kinetic pre-exponential factor (cf. Fletcher, 1958) , where dp is the dry particle diameter.

The formation free energy is accordingly calculated taking into consideration that the particles are charged. The charge-dipole interactions between the charged particles and the vapor molecules becomes significant for particle sizes smaller than 2 nm. The electrostatic attraction reduces the supersaturation required to promote nucleation as compared to heterogeneous nucleation in the case of a neutral particle. The change in Gibbs free energy during the formation of a droplet on an charged particle or cluster of atoms is given by (Thomson, 1888):

$$\Delta G = 4\pi r^2 - (4\pi/3V) r^3 kT \ln S - (ne)^2(1-1/\varepsilon)(1/8\pi\varepsilon_0)(1/r_0 - 1/r), \tag{4}$$

where r is the critical droplet radius, V is the molecular volume of the liquid, ε_0 is the dielectric constant of the condensing liquid, r_0 is the radius of the seed particle, n is the number of elementary charges carried by the particles, and e is the elementary electron charge. The first and second term express the Kelvin effect while the third term express the electrostatic interaction between the charged particle and vapor molecule. Heterogeneous nucleation probability P can then be calculated by:

$$P = 1 - exp(-J_{het} t), \tag{5}$$

where t is the residence time of the particle in the nucleation zone. Particles were considered activated when their nucleation probability exceeded 50%. Particles were considered fully wettable (i.e. vapor-particle contact angle equal to zero) and surface tension dependence on temperature was taken into account (Dean, 1999).

2.3. Supersaturation profile

A two dimensional axisymmetric model was developed in COMSOL Multiphysics simulation software, that solves the coupled heat and mass transfer equations for incompressible flow (Naiver-Stokes) for determining flow, temperature and concentration profiles of the working fluid (i.e. butanol) within the condenser (Stolzenburg & McMurry, 1991). Vapor concentration at the wall of the condenser was set equal to the saturated concentration corresponding to the wall temperature value (i.e. perfectly wetted wall). The tube walls were treated as temperature boundaries, with thermal insulation at the contact points between the saturator and condenser tube. The sheath Q_s and aerosol flow rate Q_a were fixed at 300 cm^3/min and 33 cm^3/min, respectively, resulting in a total flow rate of 333 cm^3/min in the condenser tube. All tubes had cylindrical geometry and fully developed laminar flow was assumed throughout the calculation domain. In principle, growth of activated particles can lead to a decrease of vapor concentration (vapor depletion by condensation on the seed particles) if their concentration is high, which in turn can reduce the supersaturation inside the condenser and thus decrease the detection efficiency. This process was experimentally evaluated and the effect of vapor depletion was found to be negligible and therefore not included in the model calculations (cf. Supplementary information). Although, latent heat release during condensation of vapors can reduce locally the value of supersaturation, this effect was not included in the calculations.

Under the assumption that butanol vapor behaves as an ideal gas, the partial pressure of butanol vapors can be determined by the concentration and the temperature profile calculated numerically. Fig. 1 shows a typical supersaturation profile in the condenser; only the condenser tube domain is shown here because the flow at its inlet was calculated to be saturated in butanol vapors under the specific operating conditions. Maximum supersaturation is achieved close to the centerline of the condenser tube. As a result, particles that deviate from the centerline will not be exposed to the maximum supersaturation, thereby reducing their activation and detection probability.

2.4. Particle transport losses

In order to calculate the diffusional losses of the particles within the TSI 3025 CPC, we measured the length and diameter of the five tubes through which the sampled aerosol passes. A simplified schematic layout of the entire aerosol path, along with its dimensions, is shown in Fig. 2. The diffusional losses for particles of different sizes passing through each tube were calculated using the

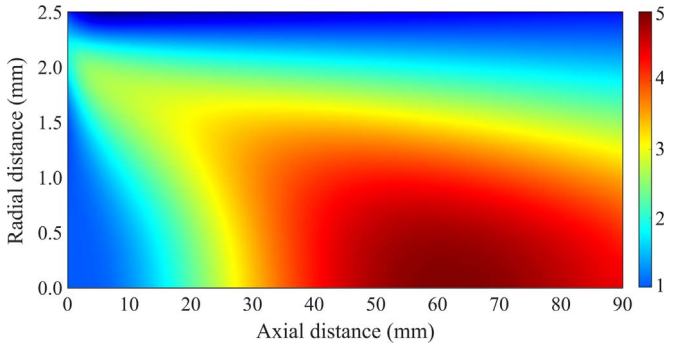

Fig. 1. Supersaturation profile developed inside the condenser tube of a 3025 TSI CPC, operated at ΔT = 32 °C, T_c = 10 °C and T_s = 42 °C.

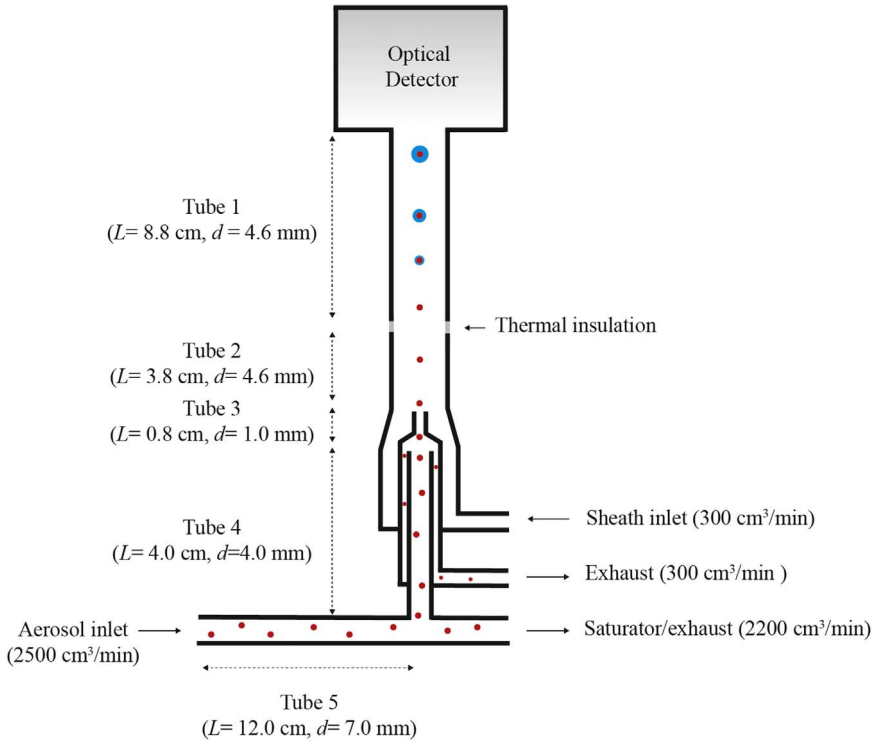

Fig. 2. Schematic layout of the TSI 3025 CPC, showing the length L and diameter d of the tubing through which the sampled aerosol flows.

well-established equation proposed by Gormley and Kennedy (1948) and appropriate values of tube geometry and flow rate.

When particles are activated inside the condenser tube (Tube 1 in Fig. 2), they grow into micron-sized droplets, for which the diffusional losses can be safely neglected. Diffusional losses in Tube 1 were calculated up to the axial point were supersaturation becomes critical for particles of a given size to activate.

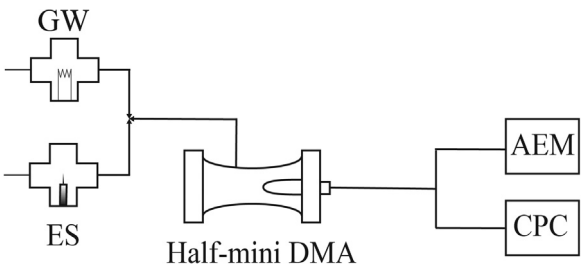

Fig. 3. Schematic layout of the experimental setup used for measuring the detection efficiency of the CPC. Key: AEM, Aerosol Electrometer; CPC, Condensation Particle Counter; ES, Electrospray Source.

3. Experimental

Fig. 3 shows the experimental setup used to measure the detection efficiency of the TSI 3025 CPC operated under a varying temperature window scheme. A custom-made electrospray source (ES; Ude & Fernández De la Mora, 2005) designed by one of us (Attoui@u-pec.fr) was used to produce tetraheptylammonium bromide (THABr; Sigma Aldrich) and tetrabutylammonium bromide (TBABr; Sigma Aldrich) ionic mobility standards for the tests. The electrospray was operated with a constant nitrogen flow through the ES chamber, and the applied pressure over the liquid solution was kept constant by using a syringe pump. This generation method produced a steady concentration of monomobile, positively or negatively charged particles covering a mobility diameter range from 0.94 to 1.73 nm.

Nickel particles larger than 2 nm were generated using a custom-made glowing wire generator GW; (Peineke, Attoui, & Schmidt-Ott, 2006). In the GW generator, high current was passed through a Ni wire, causing significant resistive heating and material evaporation from its surface. The resulting metallic vapor cloud was then cooled and diluted by a constant nitrogen flow, forming aerosol particles by nucleation and subsequent condensation.

The singly self-charged generated particles were then classified based on their electrical mobility by passing them through a high flow differential mobility analyzer half-mini DMA; (De Juan & Fernández de la Mora, 1998; Fernández de la Mora & Kozlowski, 2013; Fernández de la Mora, de Juan, Eichler, & Rosell, 1998; Kangasluoma et al., 2014; Maißer et al., 2011; Maißer, Barmpounis, Attoui, Biskos, & Schmidt-Ott, 2015; Wang et al., 2014). Mobility classification was achieved by operating the half-mini DMA at a high sheath flow rate in a closed sheath loop configuration. The half-mini DMA was calibrated using the positive monomer of the THAB particles produced by the ES. These particles have an electrical mobility Z of 0.971 Vs/cm^2 in N_2 (Ude & Fernández De la Mora, 2005).

Following classification, the concentration of the monodisperse aerosol particles at the outlet of the DMA was measured in parallel by the CPC and by an aerosol electrometer (AEM), in order to determine respectively N_{cpc} and N_{total} used in Eq. (1). The AEM consisted of a custom-made aluminum Faraday cage and a hot electrode that was connected to a sensitive electrometer (Keithley Model 6517B). In order to ensure that the particle transport losses in the tubes leading to the detectors was the same, the two parallel paths were of identical length and the sampling flow rates of both were set to 2.5 lpm. For each particle size the AEM and CPC concentration signals were recorded for a minimum of 2 min in order to monitor the stability of the concentration produced by the ES.

Detection of sub-2 nm particles is not feasible under the default operating conditions of the CPC. Two major modifications were applied to the instrument in order to increase η. Firstly, ΔT was increased from 27 °C (i.e. default operating conditions) to 32 °C in order to increase the supersaturation in the condenser tube and thus the particle activation probability. Secondly, the sheath and aerosol flows were set to 300 cm^3/min and 33 cm^3/min, respectively. Homogeneous nucleation rate at these conditions was below 1 particle per minute, at all temperature settings. In addition, the inlet sampling flow rate of the CPC was increased from its default value of 1.5 lpm to 2.5 lpm. This was done in order to reduce particle diffusional losses in the tubing from the DMA to the inlet of the CPC, and to match the flow rate of the AEM thereby ensuring equal transport losses for the two detectors. The detection efficiency of the CPC for each particle size was determined at 5 different TWs, indicated by the absolute condenser and saturator temperature in the nomenclature (e.g. TW-2–34 is the temperature window with T_c = 2 °C and T_s = 34 °C). The temperature of the optics was kept always 1 °C higher than the saturator temperature, in order to avoid vapor condensation inside the optics chamber. Table 1 summarizes the modified operating conditions as well as the experimental measurement scheme in each experiment.

In order to ensure that vapor depletion in the saturator is negligible and thus it does not affect the detection efficiencies measured at the different TWs, we performed preliminary measurements using positive THA^+ monomers (1.47 nm) at various initial concentrations. By varying the liquid-solution flow rate through the ES source we produced sample aerosols having particle number concentrations of 10^3, 10^4, and 10^5 #/cm^3, and used them to measure the detection efficiency of the CPC operated at 5 temperature window settings. At the highest concentration (i.e., 10^5 #/cm^3), the decrease of η ranged from 14.5% to 34.6% when the TW was varied from TW-2–34 to TW-10–42. When the concentration was fixed to 10^3 and 10^4 #/cm^3, however, η remained constant (within experimental uncertainty) for the different TWs (cf. Fig. S1; Supplemental information). Following these tests, all the subsequent measurements of η reported in the rest of the paper were carried out with an initial particle concentration of 10^3 #/cc.

Table 1
Summary of the modified operating parameters used for enhancing the detection efficiency of the CPC under different temperature windows. Also shown are the default operating parameters. Key: T_c, condenser temperature; T_s, saturator temperature; ΔT, temperature difference between condenser/saturator; Q_a, aerosol flow rate; Q_s, sheath flow rate.

Temperature Window	T_c (°C)	T_s (°C)	ΔT (°C)	Q_a (cm^3/min)	Q_s (cm^3/min)
TW-2–34	2	34	32	33	300
TW-4–36	4	36			
TW-6–38	6	38			
TW-8–40	8	40			
TW-10–42	10	42			
Default	10	37	27	30	270

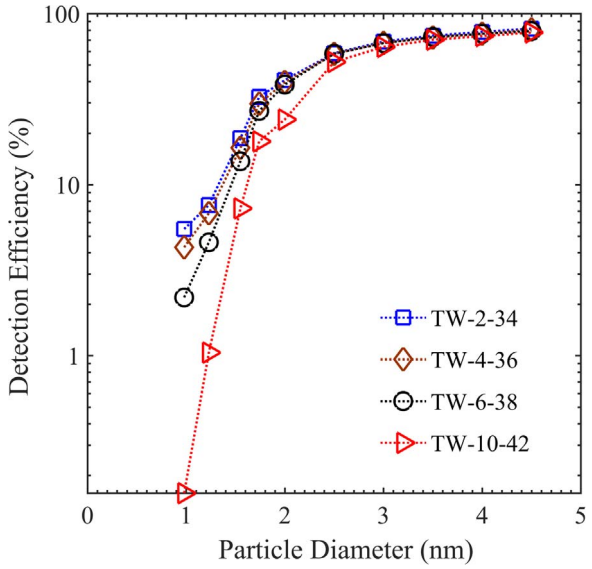

Fig. 4. Measured detection efficiency of particles having sizes from 0.94 to 4.5 nm. Each data set corresponds to a different temperature window (cf. Table 1 for the nomenclature). Dashed lines are drawn to aid the eye.

4. Results and discussion

We measured the detection efficiency of the TSI 3025 CPC operated at the TWs shown in Table 1 using particles having mobility diameters from 0.94 to 4.5 nm. The temperature difference between saturator and condenser was kept constant at 32 °C, while the temperature window was varied by changing the condenser temperature from 2 to 10 °C and the saturator temperature from 34 to 42 °C (cf. Table 1). Further reduction below 2 °C was not possible due to the limited achievable temperature range of the CPC.

Fig. 4 shows the measured η of the CPC using bromide ions (0.94 nm), positive TBABr particles (1.23, 1.55 and 1.71 nm), and positively charged Ni particles (2.5–4.5 nm). The detection efficiency clearly increased for sub-2 nm particles when the TW was shifted to lower values, whereas it remained constant for particles larger than 2.5 nm. Enhancement of η was found to increase with decreasing particle diameter. Fig. 5 shows the measured n-fold increase of η versus particle size, calculated as the ratio of η measured at the lowest and highest temperature window (i.e. η at TW-2-34 divided by η at TW-10-42), as a function of particle size. Operating the CPC at the lowest temperature window resulted in a 7-fold increase of η for the 1.23 nm, a 2.5-fold increase for the 1.55 nm, and a 1.8-fold increase for the 1.74 nm particles. The largest overall increase of η was observed for the case of the bromide ion (0.94 nm),

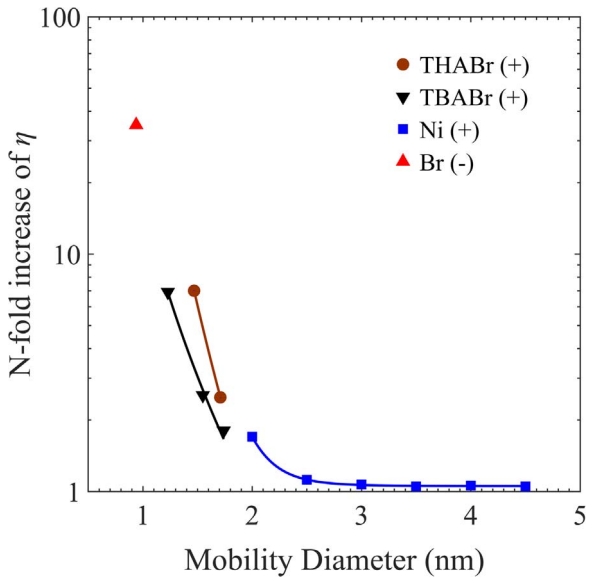

Fig. 5. Measured detection efficiency of the CPC at TW-2-34, normalized with respect to measured detection efficiency at TW-10-42. The different symbols correspond to particles of different chemical composition and charge polarity. Lines represent polynomial fits through the experimental data points.

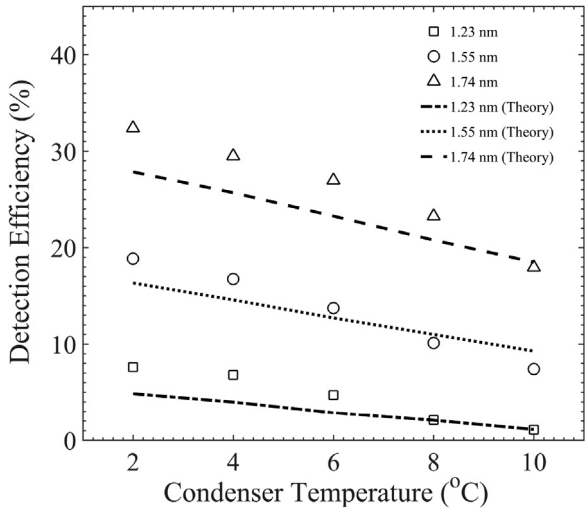

Fig. 6. Measurements (symbols) and predictions (lines) of the detection efficiency corresponding to the three positive TBABr n-mers used in our experiments. The CPC was operated at a $\Delta T = 32$ °C, with the TW being varied across 5 different positions.

which exhibited a 35-fold increase of η at the lowest temperature window (cf. Fig. 5).

It should be noted that particles of different chemical composition and polarity were used in our experiments. As shown in Fig. 5, the monomer and dimer of THABr yield detection efficiency values which are larger than those of TBABr particles, even though their mobility diameters are slightly bigger. This discrepancy can be attributed to differences in the particle chemical composition, and other physical parameters such as particle solubility, affecting heterogeneous nucleation. Although the temperature window effect described here can be used to understand differences in the activation probability of particles of similar sizes but of different composition, this is beyond the scope of this work and not investigated here any further.

Having identified that the temperature window effect becomes significant for sub-2 nm particles, we calculated the detection efficiency in that particular size range using the model described above. Fig. 6 shows the measured detection efficiency of the CPC using positively charged TBABr n-mer particles (with n = 1, 2, and 3) at different TWs (using the condenser temperature in the x-axis), in comparison with predictions from the simulations described in Section 2. Predictions and measurements agree well at TWs located at the highest temperature investigated here, but start deviating from one another as the condenser temperature is reduced. Although the differences between measurements and predictions range from 0% to 40%, qualitatively the model predicts the increasing trend of the detection efficiency with decreasing temperature window.

In order to further understand why the detection efficiency increases at lower TWs, in the discussion that follows we investigate the supersaturation profile within the condenser tube. Fig. 7a shows the supersaturation value along the centerline of the condenser

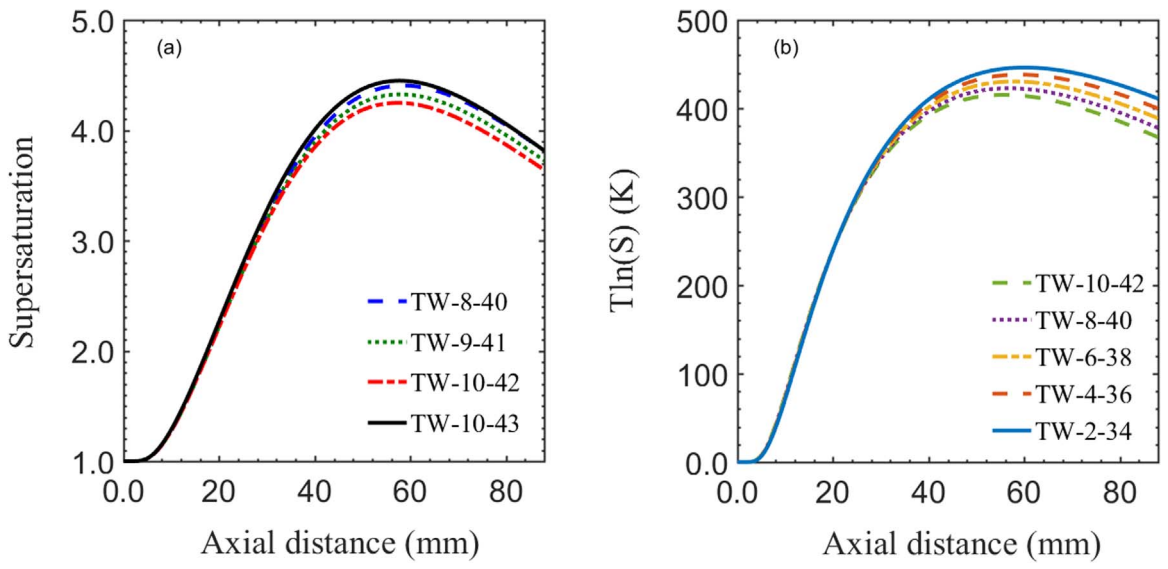

Fig. 7. (a) Supersaturation profile at the centerline of the condenser tube at 3 different temperature windows with $\Delta T = 32$ °C and one temperature window with $\Delta T = 33$ °C. (b) Tln(S) product calculated at 5 different TWs with $\Delta T = 32$ °C. The x-axis represents the distance along the centerline of the condenser tube.

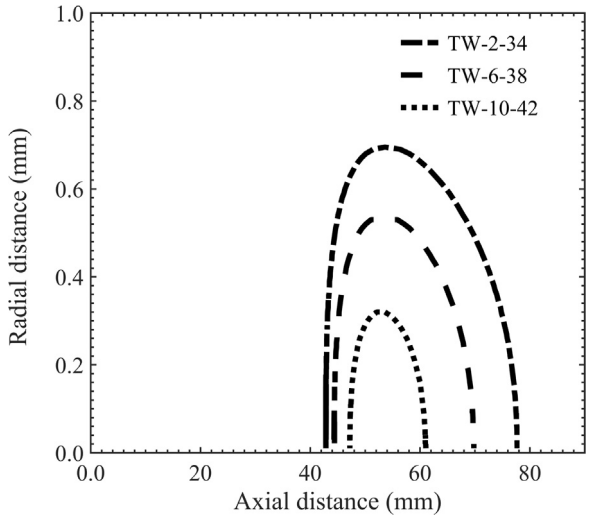

Fig. 8. Activation contours corresponding to 1.23-nm particles at three different temperature windows: TW-2-34 (dash-dotted line), TW-6-38 (dashed line), and TW-10-42 (dotted line); cf. Table 1 for details of the operating conditions.

tube for three different temperature windows (TW-8-40, TW-9-41 and TW-10-42). The peak value of supersaturation increases as the TW shifts to lower temperatures. Following Eq. (4), higher supersaturation values lower the Gibbs free energy barrier, yielding higher activation probability. On the other hand, lower temperature would decrease the Tln(S) product resulting in the opposite effect. Fig. 7b shows the calculated value of the Tln(S) for the full range of TWs used in this study. The counterbalancing effect of the lower temperature was found to be negligible. As a result, larger fraction of the sampled particles that traverse the condenser tube from the centerline will be activated at lower TWs.

Fig. 8 shows activation contours of 1.23 nm particles inside the condenser tube at three different temperature windows. The contours indicate the position at which the supersaturation has the critical value for the activation of these particles. The y-axis indicates the radial position while the x-axis indicates the axial distance along the centerline of the condenser tube. The condenser inlet is located at zero axial distance while the outlet at 8.8 cm. It is apparent that the contour area is larger for the case of TW-2-34 compared to the two other cases. Going from TW-2-34 to TW-10-42 results in a 5-fold increase of the surface area under the activation line. Assuming that the particle trajectories are not significantly influenced by the absolute temperature of the condenser, more particles will transverse the activation area in the case of the lowest temperature window settings. In addition, the activation contour for TW-2-34 is extended with respect to the axial distance compared to the TW-10-42 contour. As a result, the residence time of particles inside the growth zone is increased, leading to an increase of the detection efficiency of the CPC.

Operating the CPC at different temperature windows may prove very useful in cases where the CPC is operated in scanning temperature mode (Kangasluoma & Attoui, 2015; Kangasluoma et al., 2015). Gallar, Brock, Jimenez, and Simons (2006) and more recently Wang et al. (2015), have shown that it is possible to extract information of the size of the sampled particles by scanning the ΔT of the CPC. This effectively shifts the detection efficiency curve to large particle and thus information of particle size can be obtained by comparing differences in the concentration measurements at the different operating conditions. Scanning ΔT is usually achieved by increasing or decreasing the temperature of the saturator or the condenser.

Considering that the temperature control resolution of the 3025 is 1 °C, the user is restricted to operating the instrument with temperature increments of 1 °C, corresponding to a step in peak supersaturation. Given this limitation in temperature control, the method of scanning the TW (keeping ΔT constant) is more beneficial for sizing particles compared to scanning the ΔT. As suggested in the calculations shown in Fig. 7 that were discussed above, the resulting change in the peak supersaturation value is smaller when the scanning TW mode is used (i.e. TW-8-40, TW-9-41 and TW-10-42) compared to the scanning ΔT mode (i.e. TW-10-42 and TW-10-43). The intermediate values of peak supersaturation achieved by scanning the TW can lead to higher resolving power when the CPCs are used for particle sizing.

5. Conclusions

In this work we introduce a new controlling parameter for enhancing the detection efficiency of continuous flow CPCs. We call this parameter Temperature Window (TW), defined by the absolute value of the condenser temperature. Summarizing the key results, our investigations showed that:

- The detection efficiency of CPCs is greatly influenced not only by the temperature difference between the saturator and the condenser, but also by the absolute values of the condenser and saturator temperature. This effect is expected to influence all continuous flow CPCs operating with a working fluid whose vapor diffusion coefficient is smaller than the thermal diffusion coefficient of the carrier gas.

- A significant increase of the detection efficiency of the CPC was achieved for the sub-2 nm particles by shifting the TW to lower temperatures. The effect becomes stronger with decreasing particles size as also predicted by theory.
- By shifting the TW to lower temperatures, the peak supersaturation at the centerline is increased, while the spatial distribution of the supersaturation profile is also affected; e.g. at low TWs the effective activation surface area is increased by a factor of 5, resulting in more particles traversing regions in the saturator where they can activate.
- As the calculations show, scanning the TW could prove beneficial compared to scanning only the ΔT when using the CPC as a particle sizer, due to the finer resolution in defining the peak supersaturation inside the condenser tube.

Acknowledgements

This work was supported by NanoNextNL, a micro and nanotechnology consortium of the Government of the Netherlands and 130 partners.

Appendix A. Supporting information

Supplementary data associated with this article can be found in the online version at http://dx.doi.org/10.1016/j.jaerosci.2017.12.005.

References

Agarwal, J. K., & Sem, G. J. (1980). Continuous flow, single-particle-counting condensation nucleus counter. *Journal of Aerosol Science, 11*(*4*), 343–357.
Bricard, J., Delattre, P., Madelaine, G., & Pourprix, M. (1976). *Detection of ultra-fine particles by means of a continuous flux condensation nuclei counter.* New York: Academic Press566–580.
De Juan, L., & Fernández de la Mora, J. (1998). High resolution size analysis of nanoparticles and ions: Running a Vienna DMA of near optimal length at Reynolds numbers up to 5000. *Journal of Aerosol science, 29*(*5*), 617–626.
Dean, J. A. (1999). *Lange's handbook of chemistry.* New York: McGraw Hill.
Fernández de la Mora, J., de Juan, L., Eichler, T., & Rosell, J. (1998). Differential mobility analysis of molecular ions and nanometer particles. *TrAC Trends in Analytical Chemistry, 17*(*6*), 328–339.
Fernández de la Mora, J., & Kozlowski, J. (2013). Hand-held differential mobility analyzers of high resolution for 1–30 nm particles: Design and fabrication considerations. *Journal of Aerosol Science, 57*, 45–53.
Fletcher, N. (1958). Size effect in heterogeneous nucleation. *The Journal of Chemical Physics, 29*(*3*), 572–576.
Gallar, C., Brock, C. A., Jimenez, J. L., & Simons, C. (2006). A variable supersaturation condensation particle sizer. *Aerosol science and Technology, 40*(*6*), 431–436.
Gormley, P., & Kennedy, M. (1948). *Diffusion from a stream flowing through a cylindrical tube*. Paper presented at the Proceedings of the Royal Irish Academy. Section A: Mathematical and Physical Sciences.
Hermann, M., & Wiedensohler, A. (2001). Counting efficiency of condensation particle counters at low-pressures with illustrative data from the upper troposphere. *Journal of Aerosol Science, 32*(*8*), 975–991.
Iida, K., Stolzenburg, M. R., & McMurry, P. H. (2009). Effect of working fluid on sub-2 nm particle detection with a laminar flow ultrafine condensation particle counter. *Aerosol Science and Technology, 43*(*1*), 81–96.
Kangasluoma, J., Ahonen, L., Attoui, M., Vuollekoski, H., Kulmala, M., & Petäjä, T. (2015a). Sub-3 nm particle detection with commercial TSI 3772 and airmodus A20 fine condensation particle counters. *Aerosol Science and Technology, 49*(*8*), 674–681.
Kangasluoma, J., Attoui, M., Junninen, H., Lehtipalo, K., Samodurov, A., Korhonen, F., ... Petaja, T. (2015b). Sizing of neutral sub 3 nm tungsten oxide clusters using Airmodus Particle Size Magnifier. *Journal of Aerosol Science, 87*, 53–62.
Kangasluoma, J., Franchin, A., Duplissy, J., Ahonen, L., Korhonen, F., Attoui, M., ... Petaja, T. (2015c). Operation of the AIrmodus A11naono condensation nucleus counter at various inlet pressures,variousoperation temperatures and design of new inlet system. *Atmospheric Measurement Techniques, 8*, 8483–8508.
Kangasluoma, J., Kuang, C., Wimmer, D., Rissanen, M., Lehtipalo, K., Ehn, M., ... Petäjä, T. (2014). Sub-3 nm particle size and composition dependent response of a nano-CPC battery. *Atmospheric Measurement Techniques, 7*(*3*), 689–700.
Kousaka, Y., Niida, T., Okuyama, K., & Tanaka, H. (1982). Development of a mixing type condensation nucleus counter. *Journal of Aerosol Science, 13*(*3*), 231–240.
Kuang, C., Chen, M., McMurry, P. H., & Wang, J. (2012). Modification of laminar flow ultrafine condensation particle counters for the enhanced detection of 1 nm condensation nuclei. *Aerosol Science and Technology, 46*(*3*), 309–315.
Kulmala, M., Kontkanen, J., Junninen, H., Lehtipalo, K., Manninen, H. E., Nieminen, T., ... Rantala, P. (2013). Direct observations of atmospheric aerosol nucleation. *Science, 339*(*6122*), 943–946.
Kulmala, M., Mordas, G., Petäjä, T., Grönholm, T., Aalto, P. P., Vehkamäki, H., ... Riipinen, I. (2007). The condensation particle counter battery (CPCB): A new tool to investigate the activation properties of nanoparticles. *Journal of Aerosol Science, 38*(*3*), 289–304.
Kulmala, M., Vehkamäki, H., Petäjä, T., Dal Maso, M., Lauri, A., Kerminen, V.-M., ... McMurry, P. H. (2004). Formation and growth rates of ultrafine atmospheric particles: A review of observations. *Journal of Aerosol Science, 35*(*2*), 143–176.
Lehtipalo, K., Sipilä, M., Riipinen, I., Nieminen, T., & Kulmala, M. (2009). Analysis of atmospheric neutral and charged molecular clusters in boreal forest using pulse-height CPC. *Atmospheric Chemistry and Physics, 9*(*12*), 4177–4184.
Liu, B. Y., Whitby, K. T., & Pui, D. Y. (1974). A portable electrical analyzer for size distribution measurement of submicron aerosols. *Journal of the Air Pollution Control Association, 24*(*11*), 1067–1072.
Magnusson, L.-E., Koropchak, J. A., Anisimov, M. P., Poznjakovskiy, V. M., & de la Mora, J. F. (2003). Correlations for vapor nucleating critical embryo parameters. *Journal of Physical and Chemical Reference Data, 32*(*4*), 1387–1410.
Maißer, A., Barmpounis, K., Attoui, M., Biskos, G., & Schmidt-Ott, A. (2015). Atomic cluster generation with an atmospheric pressure spark discharge generator. *Aerosol Science and Technology, 49*(*10*), 886–894.
Maißer, A., Premnath, V., Ghosh, A., Nguyen, T. A., Attoui, M., & Hogan, C. J. (2011). Determination of gas phase protein ion densities via ion mobility analysis with charge reduction. *Physical Chemistry Chemical Physics, 13*(*48*), 21630–21641.
McMurry, P. H. (2000). The history of condensation nucleus counters. *Aerosol Science & Technology, 33*(*4*), 297–322.
Mordas, G., Kulmala, M., Petäjä, T., Aalto, P. P., Matulevicius, V., Grigoraitis, V., ... Hämeri, K. (2005). Design and performance characteristics of a condensation particle counter UF-02proto. *Boreal Environment Research, 10*(*6*), 543–552.
Peineke, C., Attoui, M., & Schmidt-Ott, A. (2006). Using a glowing wire generator for production of charged, uniformly sized nanoparticles at high concentrations. *Journal of Aerosol Science, 37*(*12*), 1651–1661.
Rosser, S., & Fernández de la Mora, J. (2005). Vienna-type DMA of high resolution and high flow rate. *Aerosol Science and Technology, 39*(*12*), 1191–1200.
Rus, J., Moro, D., Sillero, J. A., Royuela, J., Casado, A., Estevez-Molinero, F., & Fernández de la Mora, J. (2010). IMS–MS studies based on coupling a differential mobility analyzer (DMA) to commercial API–MS systems. *International Journal of Mass Spectrometry, 298*(*1*), 30–40.

Saghafifar, H., Kürten, A., Curtius, J., von der Weiden, S.-L., Hassanzadeh, S., & Borrmann, S. (2009). Characterization of a modified expansion condensation particle counter for detection of nanometer-sized particles. *Aerosol Science and Technology, 43*(*8*), 767–780.

Seto, T., Okuyama, K., De Juan, L., & de la Mora, J. F. (1997). Condensation of supersaturated vapors on monovalent and divalent ions of varying size. *The Journal of Chemical Physics, 107*(*5*), 1576–1585.

Sgro, L. A., & Fernández de la Mora, J. (2004). A simple turbulent mixing CNC for charged particle detection down to 1.2 nm. *Aerosol Science and Technology, 38*(*1*), 1–11.

Sipilä, M., Lehtipalo, K., Attoui, M., Neitola, K., Petäjä, T., Aalto, P., ... Kulmala, M. (2009). Laboratory verification of PH-CPC's ability to monitor atmospheric sub-3 nm clusters. *Aerosol Science and Technology, 43*(*2*), 126–135.

Sipilä, M., Lehtipalo, K., Kulmala, M., Petäjä, T., Junninen, H., Aalto, P., ... Riipinen, I. (2008). Applicability of condensation particle counters to measure atmospheric clusters. *Atmospheric Chemistry and Physics, 8*(*14*), 4049–4060.

Stolzenburg, M. R., & McMurry, P. H. (1991). An ultrafine aerosol condensation nucleus counter. *Aerosol Science and Technology, 14*(*1*), 48–65.

Thomson, J. J. (1888). *Applications of dynamics to physics and chemistry*. Macmillan.

Ude, S., & Fernández De la Mora, J. (2005). Molecular monodisperse mobility and mass standards from electrosprays of tetra-alkyl ammonium halides. *Journal of Aerosol Science, 36*(*10*), 1224–1237.

Vanhanen, J., Mikkilä, J., Lehtipalo, K., Sipilä, M., Manninen, H., Siivola, E., ... Kulmala, M. (2011). Particle size magnifier for nano-CN detection. *Aerosol Science and Technology, 45*(*4*), 533–542.

Wagner, P. (1985). A constant-angle Mie scattering method (CAMS) for investigation of particle formation processes. *Journal of Colloid and Interface Science, 105*(*2*), 456–467.

Wang, Y., Fang, J., Attoui, M., Chadha, T. S., Wang, W.-N., & Biswas, P. (2014). Application of Half Mini DMA for sub 2nm particle size distribution measurement in an electrospray and a flame aerosol reactor. *Journal of Aerosol Science, 71*, 52–64.

Wang, Z., Su, H., Wang, X., Ma, N., Wiedensohler, A., Pöschl, U., & Cheng, Y. (2015). Scanning supersaturation condensation particle counter applied as a nano-CCN counter for size-resolved analysis of the hygroscopicity and chemical composition of nanoparticles. *Atmospheric Measurement Techniques, 8*(*5*), 2161–2172.